

# Ameboid Microglia as a Scavenger Role in Phagocytosis of Photoreceptor Outer Segment in an Experimental Retinal Detachment Model

Manjing Cao,<sup>1,2</sup> Yahan Zhang,<sup>1,2</sup> Yan Li,<sup>3</sup> Xian Zhang,<sup>4</sup> and Mingming Ma<sup>1,2</sup>

<sup>1</sup>Department of Ophthalmology, Shanghai General Hospital (Shanghai First People's Hospital), Shanghai Jiao Tong University School of Medicine, Shanghai, China

<sup>2</sup>National Clinical Research Center for Eye Diseases, Shanghai Key Laboratory of Ocular Fundus Diseases, Shanghai Engineering Center for Visual Science and Photomedicine, Shanghai Engineering Center for Precise Diagnosis and Treatment of Eye Diseases, Shanghai, China

<sup>3</sup>Precision Research Center for Refractory Disease, Shanghai General Hospital, Shanghai Jiao Tong University School of Medicine, Shanghai, China

<sup>4</sup>Department of Ophthalmology, The Second Xiangya Hospital, Central South University, Changsha, Hunan, China

Correspondence: Manjing Cao, Department of Ophthalmology, Shanghai General Hospital, Shanghai Jiao Tong University School of Medicine, 85 Wujin Rd., Hongkou District, Shanghai 200080, China;

[mj\\_cao@sjtu.edu.cn](mailto:mj_cao@sjtu.edu.cn).

Mingming Ma, Department of Ophthalmology, Shanghai General Hospital, Shanghai Jiao Tong University School of Medicine, 85 Wujin Rd., Hongkou District, Shanghai 200080, China; [maming.ophth@sjtu.edu.cn](mailto:maming.ophth@sjtu.edu.cn).

MC and YZ contributed equally to this study and are to be considered co-first authors.

**Received:** October 8, 2024

**Accepted:** February 17, 2025

**Published:** March 4, 2025

Citation: Cao M, Zhang Y, Li Y, Zhang X, Ma M. Ameboid microglia as a scavenger role in phagocytosis of photoreceptor outer segment in an experimental retinal detachment model. *Invest Ophthalmol Vis Sci*. 2025;66(3):4.

<https://doi.org/10.1167/iovs.66.3.4>

**PURPOSE.** Photoreceptor (PR) death is the ultimate cause of irreversible vision loss in retinal detachment (RD). Previous studies have shown that microglia may have a dual role in RD. Nevertheless, the potential protective effects of microglia on PR are largely unknown. We aimed to uncover the phagocytic role of microglia in RD and propose a new concept to regulate PR survival.

**METHODS.** An RD model was conducted by injecting sodium hyaluronate into the subretinal space (SRS) of C57BL/6J wild type mice. Bioinformatics analysis was used to evaluate the highly enriched pathways and terms relating to phagocytosis in human datasets and mouse transcriptomes of RD. The observation of microglial morphology was performed by immunofluorescence through cryosection and flat mount. PLX 3397 was used for microglial ablation. Phagocytosis of the outer segment (OS) by microglia was confirmed by immunofluorescence and hematoxylin and eosin staining. Expression of phagocytic markers in microglia was detected by immunofluorescence of cryosection. The PR survival was measured by TUNEL assay and hematoxylin and eosin staining. The optical coherence tomography (OCT) images through the center of the fovea in twelve patients were obtained to observe the clinic features of IS/OS dynamics after RD.

**RESULTS.** The results showed that OS went through an accumulation-clearance process after RD. Ameboid microglia accumulated in the SRS and engulfed OS. Upregulation of phagocytic markers was observed in subretinal microglia. Depletion of microglia led to failure of OS clearance and retinal ruffling, which had the same characteristics as outer retinal undulation (ORU) in some patients with RD. PR did not benefit from microglial depletion, as no morphology and thickness recovery of PR was observed in the long term.

**CONCLUSIONS.** These results elucidate that microglial phagocytosis of OS is a critical process after RD. Insufficient phagocytosis leads to the accumulation of OS in the SRS and PR abnormalities. Appropriate regulation of microglial phagocytosis to remove OS may be a new concept to regulate photoreceptor survival.

**Keywords:** microglia, phagocytosis, outer segment (OS), photoreceptor (PR), retinal detachment (RD), outer retinal undulation (ORU)

Retinal detachment (RD) is one of the most common vision-threatening diseases worldwide. Along with rhegmatogenous RD as the primary disease, RD often serves as a complication of other retinal diseases, including proliferative diabetic retinopathy (PDR), retinopathy of prematurity (ROP), and pathological myopia.<sup>1</sup> Even though different types of RD have distinct causes, they still share some common pathological mechanisms when neurosensory

layers separate from retinal pigment epithelium (RPE). The best known and most studied is the activation of innate immune response, which is thought to be a critical cause of photoreceptor (PR) cell death.<sup>2-5</sup> As the resident immune cells in the retina, microglia are found to be activated and are the main source of inflammation, detrimental to PR.<sup>2,5</sup> However, thorough inhibition of microglia accelerates PR death, which suggests that microglia may have a dual role

in RD in that it could participate in clearance of dying PR by phagocytosis.<sup>6</sup>

In the central nervous system (CNS), microglial phagocytosis has been appreciated in its neuroprotective role for a long time.<sup>7</sup> Being the main phagocytes in the brain, microglia phagocytose neuron processes to shape neuron circuits and clear tissue debris.<sup>8,9</sup> As a part of the brain, retinal microglia show similar functions to those in the CNS, in charge of clearance of pathogens, dead cells, and protein aggregates to maintain retinal homeostasis.<sup>10</sup> Loss of phagocytic ability seen in aged microglia leads to accumulation of protein and debris, causing neuroinflammation and neurodegeneration in the retina.<sup>10,11</sup> Evidence proving the protective role of phagocytosis is reported in a dry age-related macular degeneration (AMD) model, where prevalence of RPE atrophy is more frequent in regions lacking monocytes, indicating subretinal mononuclear phagocytes may rescue RPE from death by engulfing RPE corpses.<sup>12,13</sup> Although microglial phagocytosis of dying PR in the outer nuclear layer (ONL) is observed in 24 hours post RD,<sup>6</sup> its role as a scavenger has not been explored in the late time point. Besides, our previous data have shown that the terminal station of microglia is subretinal space (SRS) adjacent to PR,<sup>2</sup> which has also been confirmed by previous studies.<sup>5,6</sup> Therefore, the phagocytosis of PR in the ONL in the first 24 hours seems more like an intermediate state for migrating microglia and it remains to uncover if the sole function of microglia consistently migrating to the SRS is to release inflammatory factors.

The structure of PR has caught our attention because PRs are neurons containing a photosensory organelle called the outer segments (OS).<sup>14–16</sup> The shedding of OS refers to the continuous generation of OS from the inner segment (IS), and tips of OS are discarded and phagocytosed by RPE.<sup>17</sup> In a healthy retina, the clearance of OS by RPE is the only way to remove the disposal of aged portions to avoid secondary cell death, inflammation, and autoimmunity.<sup>18</sup> However, the process is disturbed after the separation of the neurosensory layer and RPE layer. Structural damage of OS was observed within 12 hours after RD, after 24 to 72 hours, OS were significantly distorted.<sup>19,20</sup> OS debris shed into the SRS and was possibly phagocytosed by blood-borne cells and metaplasia RPE.<sup>21</sup> Intriguingly, the assembly of new OS continued even at 2-month RD.<sup>22</sup> A mathematical model suggested that an alternative OS removal mechanism instead of RPE was needed to explain the observed degeneration during RD.<sup>23</sup> In addition, there is a balance of disk addition and disk removal rate.<sup>23</sup> PR survival depends at least partially on the balance,<sup>23</sup> the factor of which was seldom discussed in the previous study. The physical distance provides less opportunity for RPE to engulf OS debris, whereas the location where microglia accumulate gives us a clue that they may participate in the OS removal process.

To our knowledge, there are few experiments that focus on the role of microglia involved in the OS clearance, and we also lack enough information about the OS and PR conditions after RD. In this work, we aim to study another important role of immune cells in RD and explore a new effect on PR death.

## MATERIALS AND METHODS

### Animals and Experimental Models

All animal experiments followed the guidelines of the ARVO Statement for the Use of Animals in Ophthalmic and Vision

Research and were approved by the Institutional Animal Care and Use Committee of the Shanghai General Hospital of Shanghai Jiao Tong University and Second Xiangya Hospital of Central South University. For the retinal detachment model, 8- to 10-week-old C57BL/6 mice were used for the study. The experimental model was conducted as previously described.<sup>2</sup> Briefly, after the mice were anesthetized, 3 to 4  $\mu$ L of sodium hyaluronate (Albomed, Schwarzenbruck, Germany) was injected into the SRS by a microsyringe (Hamilton, NV, USA) to make one-half of the retina detached from the RPE. Samples were collected at 1, 2, 3, 5, 7, and 14 days after RD. For the light-induced retinopathy (LIR) model, 8-week-old BALB/c male mice were used in this study. BALB/c mice were housed under a 12:12-hour light–dark cycle (7 AM on and 7 PM off). During the light cycle, light levels measured at the bottom of the mouse cages ranged from 5 to 45 lux. Induction of LIR was previously described.<sup>24</sup> Briefly, after keeping them in a dark environment overnight, the mice were exposed to 6000 lux of light for 2 hours, and then returned to their home cages under normal lighting conditions for the remainder of the experiment. The eyes were dilated with compound tropicamide eye drops (Santen Pharmaceutical Co., Ltd., Osaka, Japan) in a dark room under a red light and exposed to bright light from 10 AM to 12 PM.

### Microglia Depletion

PLX3397 (HY-16749, MedChemExpress) was formulated in AIN-76A standard chow at 1200 mg/kg following the manufacturer's instruction. C57BL/6 mice were treated with PLX3397 or control food from 2 weeks before RD until harvest.

### Human RD Retina Transcriptomic Analysis

Transcriptomic data of human RD (GSE28133) were obtained from the Gene Expression Omnibus database. Differentially expressed genes (DEGs) were identified based on fold change (FC). Hierarchical cluster analysis, heatmaps, and GO enrichment analyses of DEGs were performed using R packages (version 3.2.0). All genes in the gene set were ranked based on signal\_to\_noise. Then enrichment score (ES) was calculated with a weighted Kolmogorov–Smirnov-like statistic. The *P* value of the ES was obtained by using an empirical phenotype-based permutation test procedure. NES values were normalized enrichment scores. The FDR (false discovery rate) was used as the threshold of *P* values in multiple tests corresponding to each NES. A *P* value < 0.05 was set as the threshold for the enriched and trusted gene set.

### RNA Sequencing, Sequencing Data Extraction, and Bioinformatics Analysis

Total RNA was extracted from the mouse retinas (naïve, *n* = 3; RD at 3 days, *n* = 5), and then was purified, amplified, and labeled. Libraries were then constructed using VAHTS Universal V6 RNA sequencing Library Prep Kit (Vazyme, Nanjing, China) according to the manufacturer's instructions. The libraries were sequenced on an Illumina Novaseq 6000 platform and the read depth was around 40 million reads per sample. The clean reads were mapped to the GRCm39 reference genome (GCF\_000001635.27) using hierarchical indexing for spliced

alignment of transcripts. Fragments per kilobase millions of each gene were calculated and the read counts of each gene were obtained by HTSeq-count. Hierarchical cluster analysis, heatmaps, and GO enrichment analyses of DEGs were performed using R packages (version 3.2.0).

### Immunohistochemistry

Eyes were fixed in 4% paraformaldehyde and dehydrated in gradient sucrose PBS. Samples were sectioned at 30- $\mu$ m thicknesses. Slides were permeabilized using TBS supplemented with 0.3% Triton X-100 (BioFroxx, Guangzhou, China) for 40 minutes and then blocked in TBS-T with 1  $\times$  BSA and 10% Donkey Serum for 1 hour at room temperature. Primary antibodies included anti-CD31 (1:200, BD Biosciences), anti-iba-1 (1:500, Abcam), Rhodopsin (1:500, EnCor Biotechnology), CD68 (1:100, eBioscience), Dectin-1 (1:100, Invivogen), and DC-SIGN (1:100, R&D System). The slides were mounted with ProLong Gold Antifade Mountant (ThermoFisher Scientific, Waltham, MA, USA), and were observed under a confocal microscope (Carl Zeiss, Oberkochen, Germany; Leica, Wetzlar, Germany) with 20  $\times$  Z-stack images captured. For quantification of subretinal cells, at least three areas from each slide were chosen at random.

### Flat Mount and Skeleton Analysis

Samples were fixed in 4% paraformaldehyde for 1 hour. We washed the samples with 1X PBS, and then dissected out the retina. The block of the mouse retinas in the blocking solution contained Triton X-100. After blocking, we transferred the retinas to the primary antibodies prepared in blocking solution and incubated the retinas for 2 days. The retinas were washed in Tris-buffered saline-Tween 20 (TBST) and incubated with secondary antibodies for 2 days. After washing, we flat mounted the retinas on slides, using a dissection microscope to make four radial cuts. The slides were mounted with ProLong Gold Antifade Mountant (ThermoFisher Scientific, Waltham, MA, USA), and were observed under a confocal microscope. For cell quantification, five iba-1+ cells were randomly selected from three individual fields. The skeleton analysis was performed using the AnalyzeSkeleton plugin in ImageJ according to a published protocol.<sup>25</sup> Process length and cell size were collected from the output files.

### TUNEL Assay

Samples were sectioned at 12- $\mu$ m thicknesses. Cell death was detected using an In Situ Cell Death Detection Kit, Fluorescein (Roche, Basel, Switzerland) following the supplier's instructions. The fluorescence was detected in the range of 515 to 565 nm under microscopy.

### Histology

After fixation in 4% paraformaldehyde, the eyeballs were embedded in paraffin, sectioned into 12- $\mu$ m slices, and stained with hematoxylin and eosin. For each section, the average thicknesses of the ONL and IS/OS were calculated at 10 points of the detached region of the retina. The distances between each point were 150  $\mu$ m. The thickness

was measured using the Case Viewer application (3DHIS-TECH, Sysmex, Switzerland).

### Clinical Cases

The images were scanned by optical coherence tomography (OCT; Heidelberg, Germany) of twelve patients diagnosed with RD, which were extracted from their medical records to retrospectively observe the characteristic of the detached retinas. The study was approved by the institutional review board committees of Shanghai General Hospital.

### Statistical Analyses

The statistical analyses were performed using Prism 9 software (GraphPad Software, Inc., San Diego, CA, USA). Data are presented as the mean  $\pm$  SD. The unpaired Student's *t*-test was used to analyze experiments with only two treatments or two groups involved. One-way ANOVA analysis was used to calculate the differences among three or more groups. Significance was accepted at a *P* value of  $< 0.05$ .

## RESULTS

### Identification of Microglial Phagocytosis Through Transcriptomic Data

To find out whether alternative phagocytosis exists when the neurosensory layer of the retina separates from the RPE, we analyzed the transcriptomic data of human and mouse RD retinas. Enrichment analysis was performed with retinas from 19 patients and controls. The term "phagosome" revealed enrichment of its genes in the top 30 Kyoto Encyclopedia of Genes and Genomes (KEGG) pathways that enrich in RD (fold change  $> 2.0$ , *P*  $< 0.05$ ; Fig. 1A). Given the results of the enrichment score, we further investigated the phagocytic difference between the RD and control groups by Gene Set Enrichment Analysis (GSEA) software. If the RPE is the only phagocyte in the retina and phagocytosis ceased after RD due to downregulation of RPE phagocytosis<sup>26</sup> caused by separation, a corresponding downregulation of scavenger receptor activity should be observed in the RD retina. However, GSEA revealed the upregulation of genes in the "scavenger receptor activity" (Fig. 1B), indicating the involvement of other cells in the scavenger function. The enrichment in the "microglia pathogen phagocytosis pathway" (Fig. 1C) suggested that microglia may play an alternative phagocytic role in place of RPE. GSEA analysis of mouse retinas revealed the similar trend that genes of "phagocytosis" (Fig. 1D) and "microglia pathogen phagocytosis pathway" (Fig. 1E) enriched in RD. Previous studies suggested the possibility of microglial phagocytosis of PR, Gene Ontology-Cellular Component (GO-CC) analysis of proteins in human RD and control samples was then conducted to find evidence of clearance (Fig. 1F). Interestingly, the most enriched GO-CC was the "photoreceptor inner segment," followed by the "photoreceptor outer segment (POS)" and the "photoreceptor disc membrane," with a *P* value  $< 0.05$  (see Fig. 1F). GSEA analysis also revealed the enrichment of genes in the "photoreceptor disc membrane" (Fig. 1G) and the "POS" (Fig. 1I) in the controls, indicating the downregulation of these two components in RD, which was further identified by the heat map of those two components (Figs. 1H, 1J). The characteristics of PR discs have seldom been discussed before, but our data

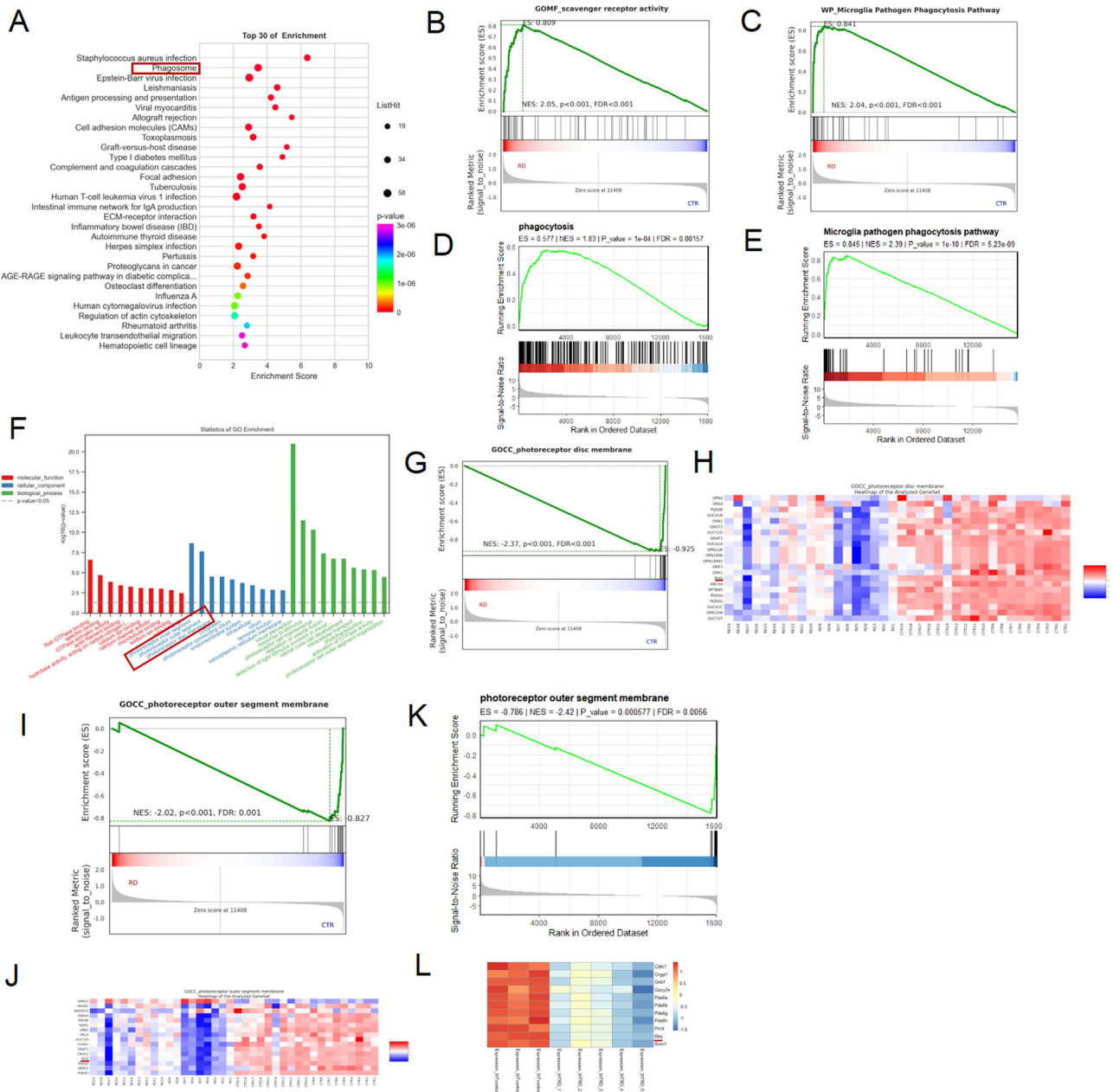


**FIGURE 1.** Positive regulation of microglial phagocytosis and negative expression of outer segments in RD were identified through transcriptomic data. (A) KEGG pathways of differentially expressed genes (DEGs) with top 30 enrichment score (fold change > 2.0,  $P < 0.05$ ) in the human dataset. Detailed results of the GSEA enrichment plot (KEGG pathways) related to microglial phagocytosis in human and mouse samples are shown in (B, C) and (D, E), respectively. (F) GO term enrichment of DEGs (fold change > 2.0,  $P < 0.05$ ). The red box highlights the most significant terms in the “cellular component (CC)” category. The GSEA enrichment plot and corresponding heat map illustrate the DEGs of the GO-CC “photoreceptor disc membrane” (G, H) and “photoreceptor outer segment membrane” (I, J) in the human dataset and “photoreceptor outer segment membrane” (K, L) in the mouse dataset. Rhodopsin (Rho) was found to be significantly negatively regulated in RD (H, J, L, highlighted by the red line).

proposes an evitable change in PR discs after RD. The same enrichment was also shown in mouse transcriptomic data (Figs. 1K, 1L). Taken together, the DEG analysis suggested that microglia actively engaged in phagocytosis and might be responsible for the PR disc clearance after RD.

### Morphology and Location Changes of Microglia Following RD

First, we observed the morphological change of microglia and the location of their assembly. To identify microglia

at different layers of the retina, sections were co-stained with Iba-1 and CD31 (CD31 as a blood vessel marker). A representative image of individual microglia was provided to demonstrate their morphology. Microglia showed typical activated morphology, including fewer branches and shorter processes in both the superficial layer (Figs. 2A–D) and the deep layer (Figs. 2F–I) from 24 hours to 3 days following RD, and then displayed the trend of recovery at 7 days after RD (Figs. 2E, 2J). The number of branches and microglial size were quantified and shown in Figure 2P and Figure 2Q, respectively. Microglia around the deep vasculature revealed fewer branches (Fig. 2P), and tighter

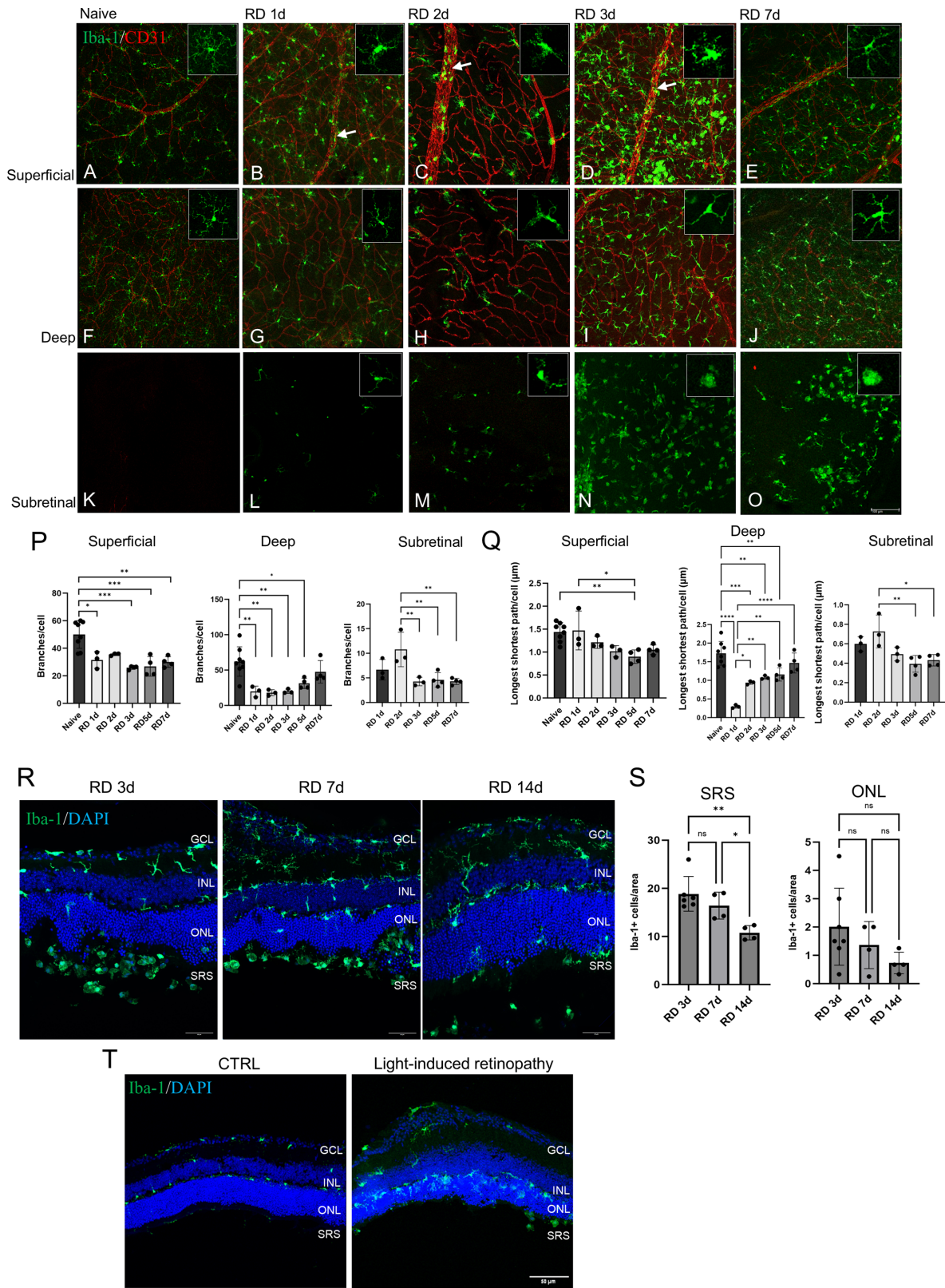


**FIGURE 2.** The morphological characteristics and location features of microglia reveal their activation and possible phagocytic function. (A–O) Representative flat mounts showing microglia in the indicated layers of retina from control mice and mice at days 1 to 7 post-RD. Representative image of single microglia at each layer was shown on the right angle. The superficial layer (from GCL to INL), deep layer (from INL to OPL), and subretinal space are classified based on the CD31 staining. The *white arrows* indicate the relationship between blood vessels and circulating monocytes. Scale bars = 100 μm. Quantification of process length and relative cell size (longest shortest path) of Iba-1+ cells in the superficial layer and deep layer were shown in (P) and (Q). (Naive, n = 8; 1, 2, and 3 days after RD, and n = 3; 3, 5, and 7 days after RD, n = 4.) (R) Representative immunofluorescence images of microglial reactivity and dynamic movement in cross-sections of the retinas at 3, 7, and 14 days after RD. For immunofluorescence, Z-stack images of the entire thickness of the retina were created. Scale

bars = 50  $\mu\text{m}$ . (S) Quantification of microglia in the SRS and ONL at different time points after RD. (3 days after RD,  $n = 6$ ; 7 days after RD,  $n = 4$ ; and 14 days after RD,  $n = 4$ ). (T) Representative immunofluorescence images of microglial reactivity in cross-sections of retinas of control (CTRL) and light-induced retinopathy. Statistical analysis: (P, Q, S) the 1-way ANOVA followed by Tukey's multiple comparison.  $^*P < 0.05$ ,  $^{**}P < 0.01$ ,  $^{***}P < 0.001$ ,  $^{****}P < 0.0001$ .

cell bodies (Fig. 2Q) compared with those around the superficial vasculature. The reason for this phenomenon may be attributed to the fact that the location of microglia in the deep retina may have allowed their quick reactivation and movement to the SRS prior to the microglia in the superficial layer. Furthermore, decreased numbers of microglia in the deep layers (Figs. 2G, 2H) were obvious at the acute phase of RD, whereas the circulating monocytes started to invade in the superficial layers (Figs. 2B–D, white arrow). On day 7 following RD, microglia acquired more ramified morphologies in both the superficial and deep layers of the retina (see Figs. 2E, 2J), and the empty niche of microglia in 1- and 2-days post RD was filled in. Microglia started to present in the SRS 1 day after RD and took on an obvious amoeboid morphology from 3 days to 7 days after RD (Figs. 2L–O). The subretinal microglia exhibited the morphology most similar to that of an amoeboid (see Figs. 2M–O) and the fewest branch numbers (Fig. 2P). The cross section of the retina better exhibited the location of microglial accumulation (Fig. 2R). Most of the Iba-1+ cells gathered in the SRS, were almost 10 times greater than those in the ONL layer (Fig. 2S). In contrast to the light-induced retinopathy model, which showed microglial accumulation in the ONL layer to phagocytose dying PR nuclei (Fig. 2T), microglia in the RD demonstrated distinct locations of accumulation. The number of microglia in the SRS and ONL peaked at 3 days after RD, and decreased at 7 and 14 days following RD (see Fig. 2S). Taken together, the data above show the dynamic of microglial activation and morphological change in response to RD. The presentation of amoeboid microglia in the SRS indicates the possibility of their phagocytic function.

### The Association Between Microglia and Photoreceptor Outer Segments

Given the evidence of microglial recruitment in the SRS, where the POS are located, we further investigated the underlying relationship between microglia and POS (marked by rhodopsin). In the attached retina, the structure of OS is densely organized (Fig. 3E), with the circular fluorescence of the OS being only detected at the terminal tip (Fig. 3A). However, at 3 days after RD, the OS accumulated disorderly in the SRS (Figs. 3B, 3F), suggesting insufficient phagocytosis by RPE. Interestingly, circular fluorescence of the OS colocalized with Iba-1+ cells (see Fig. 3B, white arrow). At 7 days after RD, the density of OS significantly decreased (Figs. 3C, 3G). Overlapping of OS and Iba-1+ cells was obviously identified (see Fig. 3C, yellow arrow), suggesting the debris of OS tightly attached to the subretinal microglia. Hematoxylin and eosin staining also revealed a similar pattern of OS aggregating around the subretinal cells (see Fig. 3G, yellow arrow). At 14 days after RD, OS degenerated along with the thinner of ONL, whereas fewer microglia presented compared with the previous time points (Figs. 3D, 3H). The decreased volume of OS with time in the detached retina indicated that there may be a mechanism responsible for OS clearance. In addition, the relationship between the microglia and the OS gave us a clue that the

microglia may have a scavenger role in the SRS. The enlarged image showed a better view of OS bound to Iba-1+ cells in the SRS (Fig. 3I). Overall, microglia in the SRS may contribute to OS clearance.

### Phagocytic Marker Is Identified in Subretinal Microglia

To identify the phagocytic activation of subretinal microglia, the markers that were reported to participate in phagocytosis were examined, including CD68, Dectin-1, and dendritic cell-specific ICAM grabbing non-integrin (DC-SIGN).<sup>27,28</sup> Immunopositivity of CD68, Dectin-1, and DC-SIGN was observed in the subretinal microglia (Figs. 4A, 4D, 4E, Supplementary Figs. S1A, S1B) at different time points after RD. The immunofluorescence of CD68, Dectin-1, and DC-SIGN was exclusively observed in cells with amoeboid morphology in the SRS and ONL, whereas no immunofluorescence was detected in the inner retina layers or the naïve retina (see Figs. 4A, 4D, 4E). In the light-induced retinal degeneration model, Iba-1+CD68+ cells were mainly in the ONL (Fig. 4B), which confirmed our hypothesis that in the RD model, the microglia performed phagocytosis mainly in the SRS. The number of Iba-1+CD68+ cells decreased with time after RD, whereas the number of Iba-1+CD68– cells increased (Fig. 4C), indicating that the phagocytic function of the subretinal cells may not be constant all the time. The upregulated phagocytic marker observed in subretinal microglia showed their active engagement in phagocytosis after RD.

### Depletion of Microglia Leads to Failure of OS Clearance

To determine whether the OS clearance after RD is microglial phagocytosis dependent, we used PLX3397 to deplete microglia. The administration of PLX3397 did not change the morphology of the naïve retina, including the PR-RPE interface (Supplementary Figs. S2A, S2B). Colocalization of Iba-1 and rhodopsin at 7 and 14 days after RD was observed in mice treated with control food, as previously described (Figs. 5A, 5B, control food). Interestingly, the absence of microglia led to the accumulation of round OS discs in the SRS (see Figs. 5A, 5B, PLX3397 food). By keeping the antibody concentrations and microscope settings constant, the fluorescence of OS was measured in a quantitative way. The total area of OS in the retina with PLX food was approximately 1.5 times greater than that of control food at two different time points after RD (Fig. 5C). The occupied area of OS at 14 days (see Fig. 5B, PLX3397 food) after RD was considerably larger than it was at 7 days (see Fig. 5A, PLX3397 food, Fig. 5C), and the shape of OS exhibited a looser and more dispersed pattern at later time points (see Fig. 5B, PLX3397 food). The fluorescent intensity of OS was also significantly stronger in the absence of microglia (Fig. 5D). However, there was no statistical difference in the intensity of OS with microglial depletion at 7 or 14 days after RD. PR may have encountered considerable mortality

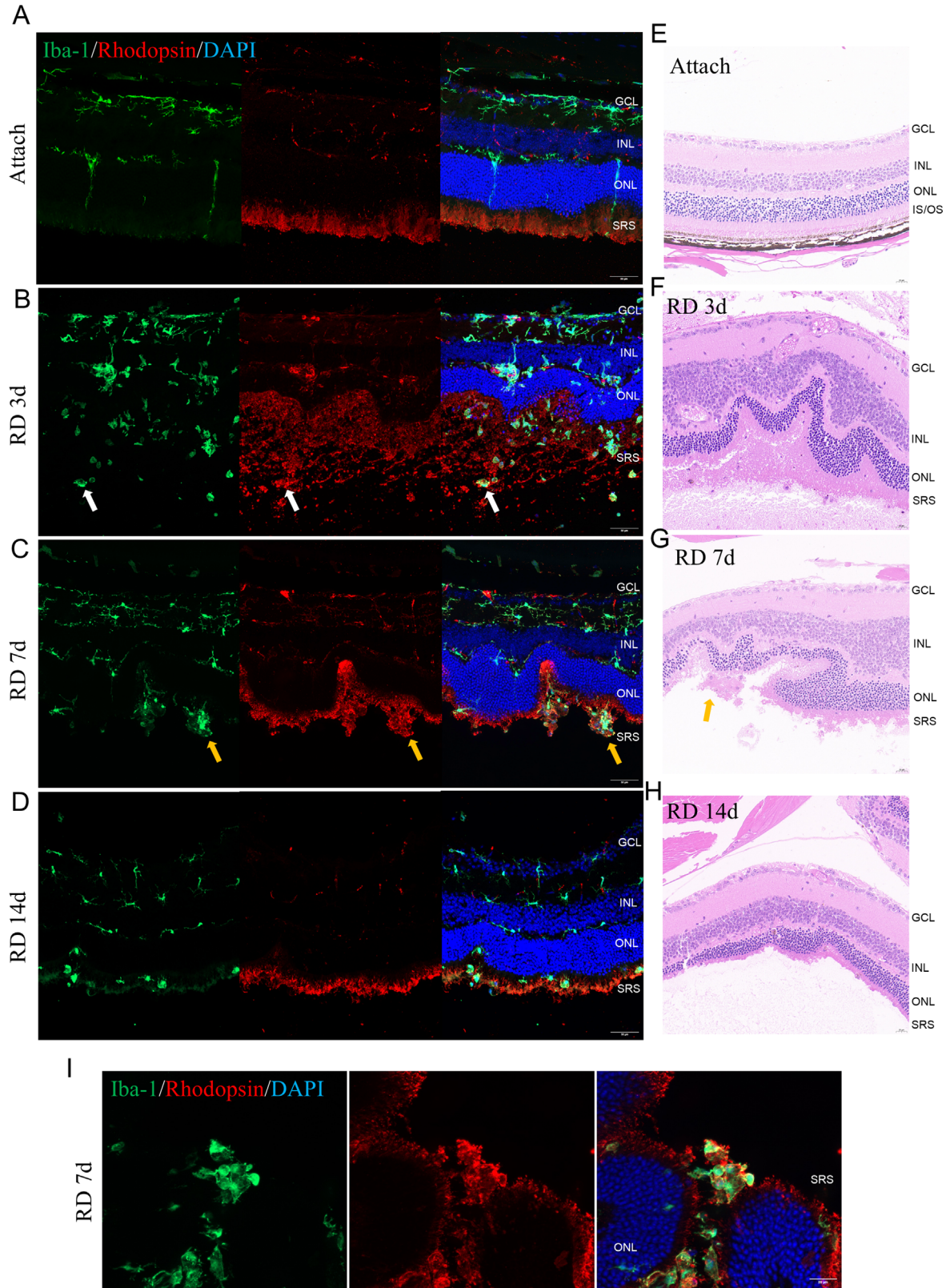


**FIGURE 3.** Outer segment dynamics and microglial phagocytosis after RD. Representative immunofluorescence images of Iba-1 and Rhodopsin colocalization in cross-sections of retinas in (A) attached area (as control) and the detached area at (B) 3, (C) 7, and (D) 14 days after RD. The *white* and *yellow arrows* highlight representative cells of colocalization. Scale bars = 50 μm. Representative hematoxylin and eosin staining images of retinas in (E) attached area (as the control) and the detached area at (F) 3, (G) 7, and (H) 14 days after RD. Scale bars = 20 μm. Magnification of image (I) showing substantial colocalization of the microglia (*green*) and the outer segment (*red*). Scale bars = 20 μm.

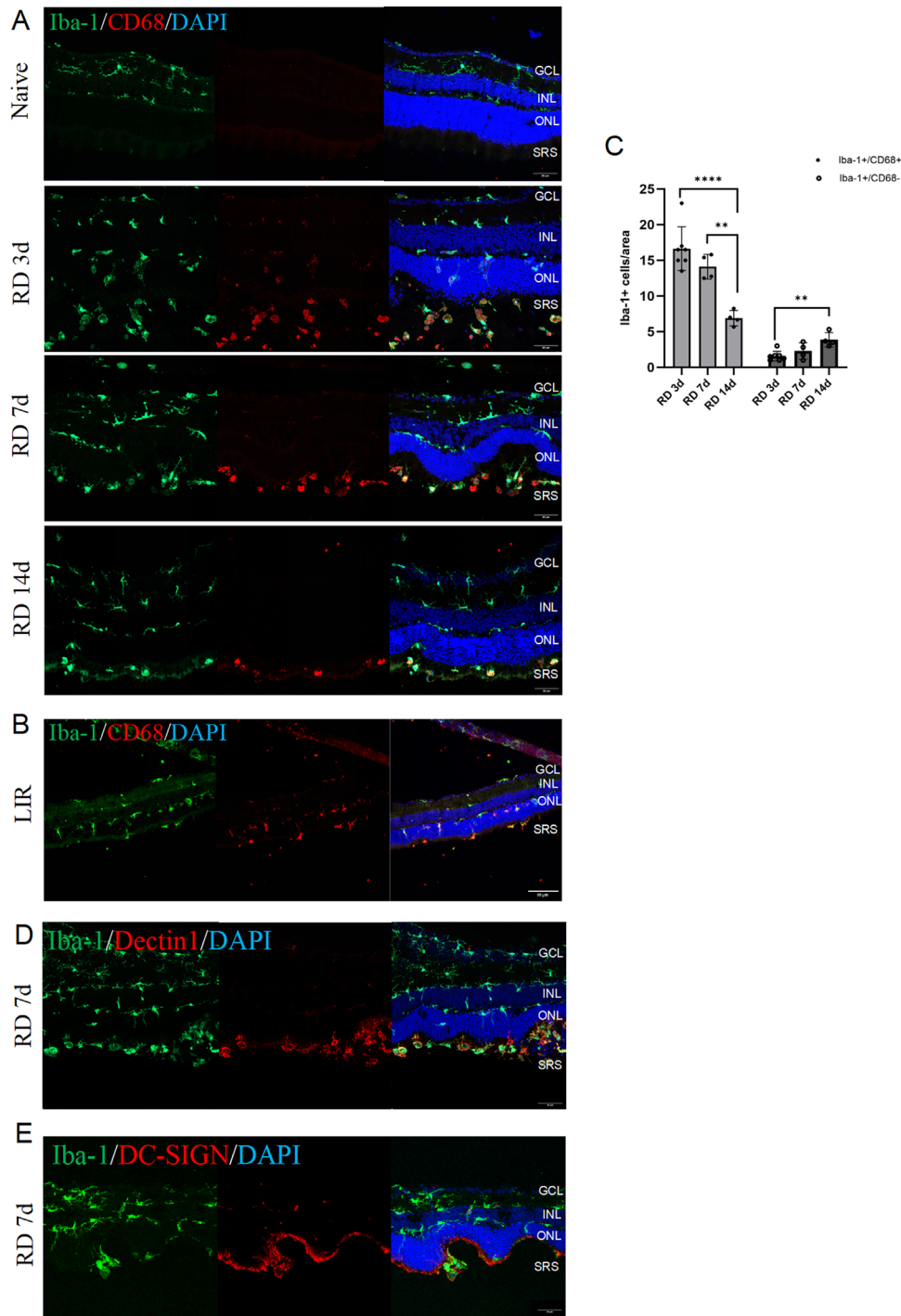


**FIGURE 4.** Upregulated phagocytic function in subretinal microglia. (A) Representative images from cross-sections stained with Iba-1 and CD68 at 3, 7, and 14 days after RD, with (A) Naïve and (B) LIR model as the control. Scale bars = 50  $\mu$ m. (C) Quantifications of Iba-1+CD68+ and Iba-1+CD68- cells related to (A) (3 days after RD,  $n = 6$ ; 7 days after RD,  $n = 4$ ; and 14 days after RD,  $n = 4$ ). Representative images from cross-sections stained with Iba-1 and (D) Dectin1/ (E) DC-SIGN at 3 days after RD ( $n = 4$ ). Scale bars = 50  $\mu$ m. Statistical analysis: (C) 1-way ANOVA followed by Tukey’s multiple comparison. \* $P < 0.05$ , \*\* $P < 0.01$ , \*\*\* $P < 0.001$ , \*\*\*\* $P < 0.0001$ .

14 days post-RD, potentially explaining the reduced ONL thickness and diminished rod disc assembly rates. The result is further confirmed by hematoxylin and eosin staining. In comparison to the control food, round OS discs gathered in the SRS in the PLX3397 group (Fig. 5G), indicating a failure in OS clearance (Fig. 5H). The TUNEL assay was performed to evaluate the effect on PR in the absence of microglia

in the acute phase (see Fig. 5E). The reduced number of TUNEL+ cells in ONL indicated that PR benefited from the ablation of microglia (Fig. 5F). However, after 14 days of RD, the thickness of ONL with microglial depletion was slightly thinner than the controls, implying the ablation of microglia actually accelerated PR death in the following time, which negated the initial rescue of PR (Fig. 5I). Furthermore, the

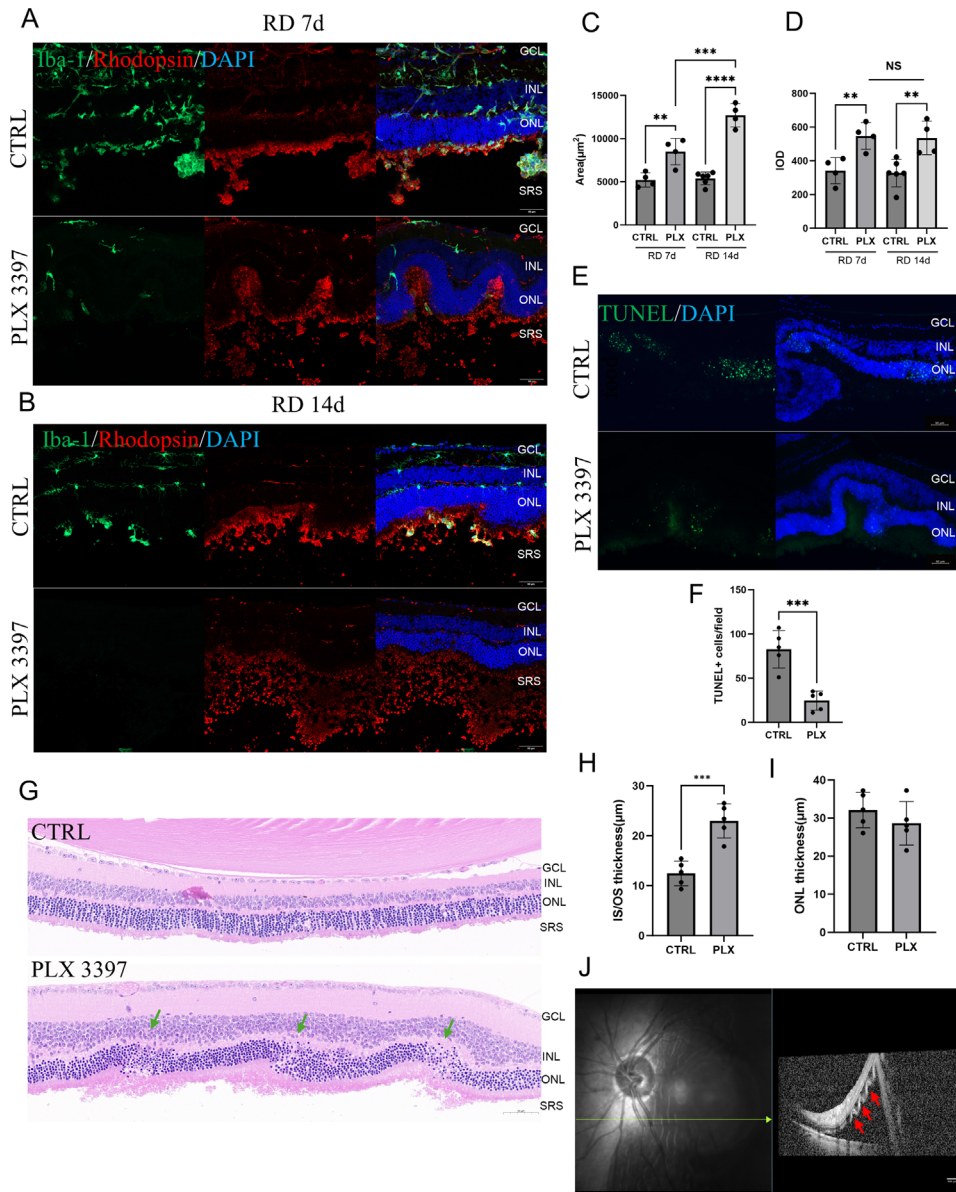


**FIGURE 5.** Ablation of microglia led to OS accumulation in the SRS and accelerated PR death. Representative images from cross-sections stained with Iba-1 and Rhodopsin of retinas treated with control food (CTRL) and PLX3397 food at (A) 7 and (B) 14 days after RD. Scale bars = 50 µm. Quantifications of (C) area and (D) fluorescent density related to (A) and (B) (7 days after RD, CTRL and PLX:  $n = 4$ ; and 14 days after RD, CTRL:  $n = 6$ , PLX:  $n = 4$ ). (E) Representative immunofluorescent images of TUNEL+ cells in ONL of RD retinas treated control food (CTRL) and PLX3397 food at 3 days after RD. Scale bars = 50 µm. Quantifications of (F) TUNEL+ cells related to (E) (CTRL,  $n = 5$ ; and PLX3397,  $n = 5$ ). (G) Representative hematoxylin and eosin staining images of retinas treated with control food (CTRL) and PLX3397 food at 14 days after RD. Scale bars = 50 µm. The green arrows mark the abnormal morphology of ONL and ruffling retina. Quantifications of (H) IS/OS thickness and (I) ONL thickness related to (G) ( $n = 5$ ). (J) An OCT image demonstrates an outer retinal undulation (ORU) in a patient with 14 days of RD. Scale bars = 500 µm. The ORU defined as three combinations of negative and positive undulations, was marked by the red arrows. Statistical analysis: (C, D) 1-way ANOVA followed by Sidak's multiple comparison, (F, H, I) unpaired  $t$ -test. \* $P < 0.05$ , \*\* $P < 0.01$ , \*\*\* $P < 0.001$ , \*\*\*\* $P < 0.0001$ .

nucleus in the ONL exhibited abnormal morphology in the mice treated with PLX food (see Fig. 5G, green arrows). One more interesting finding is that stacks of OS are always related to retinal ruffling, which is observed at some time points of RD (see Figs. 3F, 3G), and more often seen in the PLX group (see Figs. 5G, 6D). The ruffling retinas had similar characteristics with outer retinal undulation (ORU) in some RD patients (see Fig. 5H, red arrows). The ORU was reported to be predictive of poorer visual acuity.<sup>29</sup> Thus, our data demonstrated that the depletion of microglia resulted

in the failure of OS clearance and may accelerate the death of PR.

### The Ratio of IS/OS and ONL Thickness: A Promising Indicator Reflecting the Phagocytic Efficiency

The aforementioned data suggested that microglia participated in the clearance of subretinal OS, and the absence of

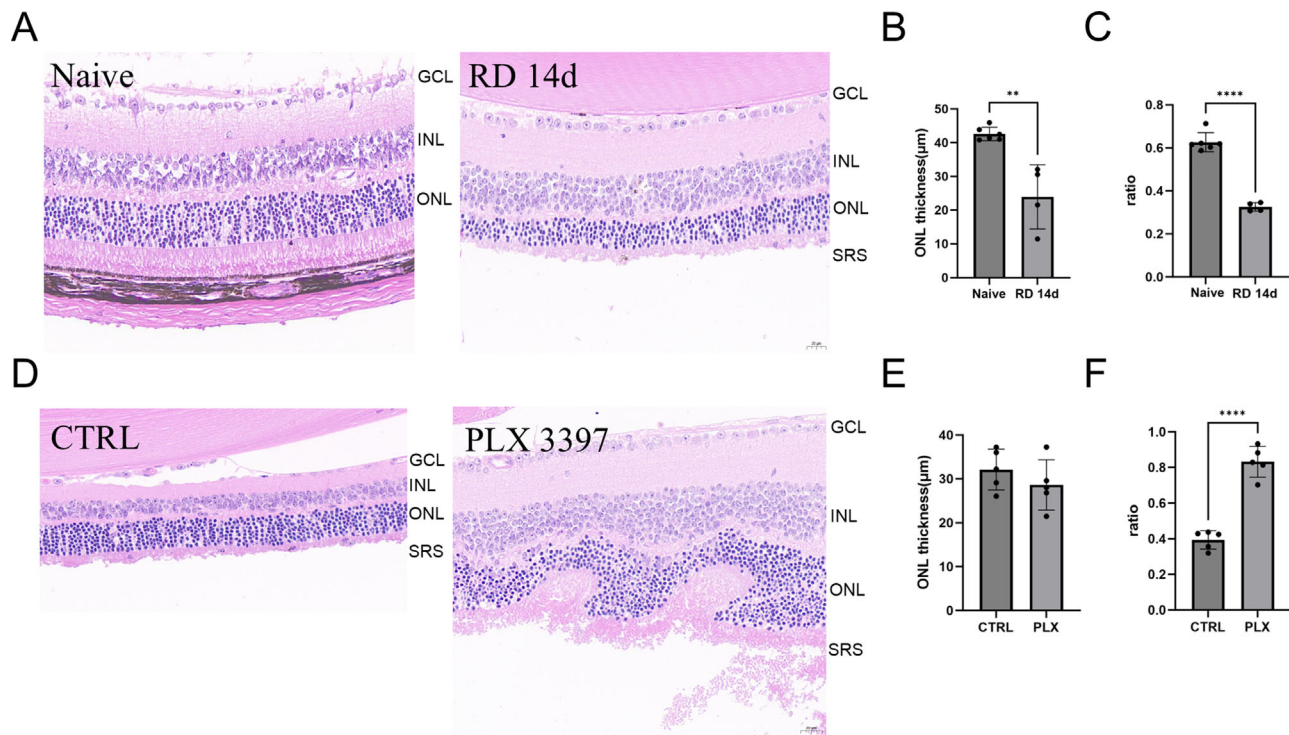


**FIGURE 6.** The increased ratio of IS/OS and ONL thickness as an indicator reflecting insufficient phagocytosis. (A) Representative hematoxylin and eosin staining images of retinas of naive and 14 days after RD. Quantifications of (B) ONL thickness and (C) ratio related to (A). (D) Representative hematoxylin and eosin staining images of retinas treated with control food (CTRL) and PLX3397 food at 14 days after RD. Scale bars = 20  $\mu\text{m}$ . Quantifications of (E) ONL thickness and (F) ratio related to (D). Statistical analysis: (B, C, E, F) Unpaired *t*-test.  $**P < 0.01$ ,  $****P < 0.0001$ .

this scavenger did not contribute to PR rescue but rather expedited PR death. We hypothesize that a balance of OS disc generation and clearance is essential to PR survival, even during RD. The OS is generated by PR, consistently cleared by phagocytes. Therefore, under normal circumstances, the ratio of OS versus PR is supposed to be homeostatic and constant. In that case, an appropriate indicator that can assess the dynamics of OS and estimate the proper phagocytic efficiency after RD is needed. Because hematoxylin and eosin staining best conserved the morphology of retina, we measured the ratio based on the hematoxylin and eosin image. In the naive retina, the OS was engulfed by RPE, preserving the ratio as the ideal ratio to maintain PR homeostasis (Fig. 6A). At 14 days after RD, the ratio decreased dramatically when the microglia were present (see Figs. 6A, 6C). This may be because of the death of PR (Fig. 6B) and depression of the OS generation. In the PLX group, the quantity of PR cells (indicated by ONL thickness) was lower than that in the control group (Fig. 6E). However, the ratio increased significantly (Fig. 6F), suggesting insufficient clearance of OS, as the removal rate of OS is considerably slower than the addition rate. Taken together, analyzing the thickness of ONL and the ratio together could give us a straightforward quantitative description to help regulate the removal rate of OS by mediating phagocytes in future research.

### Extrapolation to the Clinic

To extrapolate findings from the animal model to assess the possible correlation with clinical characteristics of rheg-

matogenous retinal detachment (RRD), we observed the OCTs of patients with RD at different time points. The white dashed lines were added to better demonstrate the boundaries between the inner retinal layers and the outer retinal layers. Compared with the intact and highlighted signals of the outer retinal layers (including Myoid zone, Ellipsoid zone, and OS) in the attached retina (Fig. 7, yellow arrows), the thicker outer retinal layers were found in the detached area. From 3 days to 1 month after RD, the IS/OS layer was obviously chunkier than the ONL. From 2 months to 6 months, the thickness of the IS/OS layer was no thicker than the ONL. For patients with 1-year RD, marked thinning of the ONL and IS/OS layer was found. At different time points, hyper-reflective foci appeared in the SRS, which could be infiltrating microglia. Furthermore, we measured the ratio of IS/OS to ONL thickness in a group of patients with 5 to 60 days of RD and found a greater ratio than in the fellow eye (see Fig. 7H), indicating a decreased clearance of OS without RPE after RD. To preliminarily explore the correlation of the ratio (IS/OS to ONL) to best-corrected visual acuity (BCVA), we follow two patients after scleral buckling surgery (Figs. 7I, 7J). Interestingly, after the surgery, the ratio (IS/OS to ONL) decreased whereas the BCVA continued to improve, despite the persistent macular detachment, supporting our hypothesis. To note, the peak time of phagocytosis may be different between various species. Therefore, the morphology of OS and microglia seems dissimilar between human and mouse at the same time points. However, the tendency of morphological changes of outer retinal layers seemed similar.

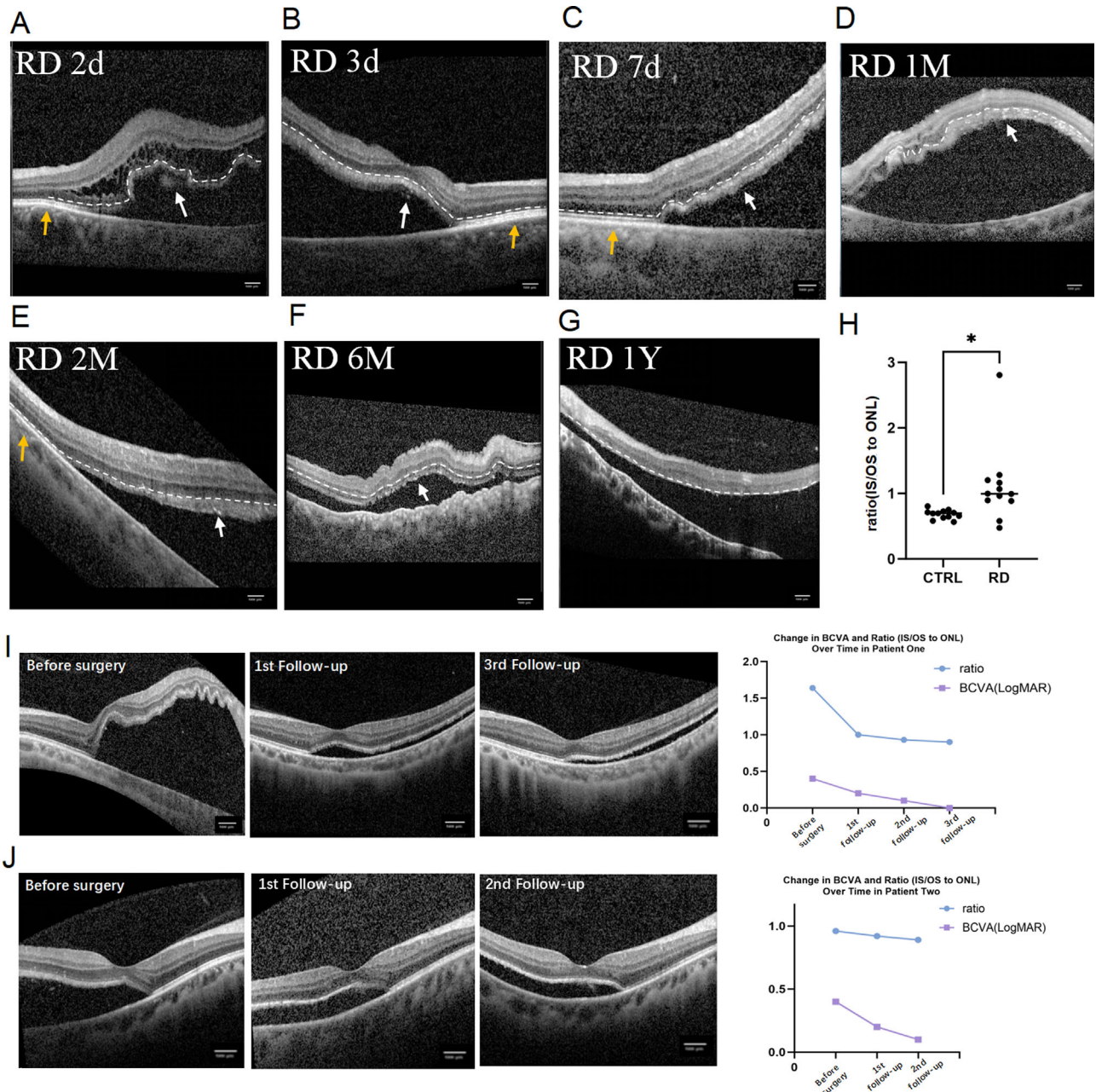


**FIGURE 7.** Representative OCT images showing detached retinas of patients at 2 days, 3 days, 7 days, 1 month, 2 months, 6 months, and 1 year after RD. The concise information of each patient diagnosed with rhegmatogenous retinal detachment (RRD) in OCT scans. **(A)** The image is from a 58-year-old male patient diagnosed with RD after 2 days of blurred vision with dark floaters. **(B)** The image is from a 71-year-old female patient diagnosed with RD after 3 days of blurred vision with dark floaters. **(C)** The image is from a 38-year-old female patient diagnosed with RD after 7 days of vision loss with a shadow in the right field. **(D)** The image is from a 72-year-old female patient diagnosed with RD after 1 month of blurred vision. **(E)** The image is from a 19-year-old male patient diagnosed with RD after 6 months of blurred vision. **(F)** The image is from a 72-year-old female patient diagnosed with RD after 2 months of blurred vision. **(G)** The image is from a 17-year-old female patient diagnosed with RD after 1 year of blurred vision. No systemic diseases are reported in all the patients. The *yellow arrows* mark the attached retina, whereas the *white arrows* mark the detached retina. The *white dashed lines* are drawn along the external limiting membrane (ELM) to better indicate the boundary of outer retinal layers and inner retinal layers. The difference in thickness of outer retinal layers between attached and detached regions exhibits the morphology change of the outer retina separated from RPE. **(H)** Quantifications of the ratio of IS/OS versus ONL in the RD eye compared to the fellow eye. The study used an unpaired *t*-test for statistical analysis, with a significance level of less than 0.05. **(I)** The series of macular OCT images shows the tendency of the ratio (IS/OS to ONL) in the retina before and after scleral buckling surgery in a 23-year-old man. The first, second, and third follow-ups were 3 weeks, 7 weeks, and 11 weeks after surgery, respectively. The line graph illustrates how the ratio (IS/OS to ONL) tends to align with BCVA over time. **(J)** The series of macular OCT images shows the tendency of the ratio (IS/OS to ONL) in the retina before and after scleral buckling surgery in a 31-year-old woman. The first and second follow-ups were 1 week and 5 weeks after surgery, respectively. The line graph shows the tendency of ratio (IS/OS to ONL) is in accordance with BCVA across the time. Scale bars 500  $\mu$ m.

## DISCUSSION

This study provides a novel understanding of microglial participation in the RD process. Our results showed that separation of PR and RPE caused the accumulation of OS in the SRS, microglia served as important phagocytes to clear the subretinal OS. Pharmacological microglial ablation led to the failure of OS clearance in the SRS, which accelerated PR death. We also proposed that regulation of microglial phagocytosis to remove OS may be a new concept to regulate PR survival.

Microglia participate in the pathological process of RD, and previous studies focused on their inflammatory function in promoting PR death.<sup>2,5</sup> The inflammatory cascade induced by microglia was detrimental to PR in the acute phase after RD. Therefore, inhibition of microglial activation and inflammation at an early time was shown to be protective to PR.<sup>2,5,30</sup> However, the long-term advantages of microglial depression for PR are rarely reported. In our previous study, we found that long-term suppression of microglia could negate the beneficial effect on PR.<sup>2</sup> Thus, we proposed a hypothesis that microglia may play a dual role in RD. The dual roles of microglia have been discussed in various diseases. As exemplified in a multiple sclerosis model, microglia are found to change from toxic to protective roles during different phases of the disease.<sup>31</sup> Over-activated microglia may lead to neuronal damage, but they can also release protective factors or remove pathogens to repair tissue at the late phase of disease.<sup>32–34</sup> Microglia may also have a similar change in function in RD. Thus, if we only focus on the inflammatory facet of microglia, we may neglect the possible reason for failure of anti-inflammatory therapies.

To elucidate the potential function of microglia, the transcriptomic data of human and mouse RD retinas were performed to uncover the upregulation of microglial phagocytosis in the RD retina. The flat mounting of the retina helped to take a closer look at the morphological change of microglia after RD, which provided the potential roles reflecting their physiological functions.<sup>35</sup> The “microglial activation” was observed in the superficial and deep retina vasculature, including retraction of processes and compaction of cell bodies after RD. However, the subretinal microglia exhibited a remarkable amoeboid morphology distinct from intraretinal, as an indication of their phagocytic capacity.<sup>35,36</sup> In the CNS, the fully retracted processes of microglia were related to their phagocytic activity<sup>37</sup> in response to the presence of pathological insults.<sup>38</sup> Amoeboid microglia facilitate the removal and degradation of endogenous or exogenous insults by phagocytosis, and the successful removal of pathogens contributes to the recovery in the CNS.<sup>39</sup> In the context of RD, the phagocytosis of injured or dying PR by microglia has been reported in the ONL within 24 hours of RD.<sup>6</sup> Despite the presence of microglia in the ONL, our observations revealed that the majority of amoeboid microglia were located in the SRS at later time points. The phenomenon is different from the light-induced retinopathy model, in which most microglia infiltrated and phagocytosed the PR body in the ONL.<sup>40</sup> The location of subretinal microglia in RD indicates they may phagocytose different pathogens, or there are stronger “Eat me” signals to attract microglia to the SRS. Gene enrichment in the GO-CC “photoreceptor outer segment membrane” and the presence of subretinal microglia gave us a clue about the possible deposits that microglia cleared.

The concept of OS shedding was brought to light back in the 1900s.<sup>41</sup> The turnover of OS is determined by two processes, including the generation of new disc membranes and the removal of old disc membranes by RPE.<sup>42,43</sup> In general, the amount of shed membrane equals the amount of newly added membrane, resulting in a constant length for PR and their discs in homeostasis.<sup>42</sup> However, there has been limited discussion of the dynamics of OS shedding in RD. Because rods are the major type in mammalian retinas (including humans), we immunolabeled the rhodopsin in rod OS to observe OS dynamics.<sup>44,45</sup> A previous study showed that within 12 hours of RD, the structure of OS shows a damaged pattern.<sup>19</sup> Our data revealed abnormal OS structures at various time points after RD. The amounts of OS exhibit a fluctuating pattern like a roller coaster. Massive amounts of OS accumulated in the SRS at 3 days after RD, without routine and efficient removal by RPE. Then, the OS was phagocytosed by subretinal microglia, leading to a significant decrease in the total volume of OS at 14 days after RD. The results in our study answer part of the hypothesis in a published article that microglial phagocytosis serves as an alternative removal mechanism that existed in replacement of RPE during RD.<sup>23</sup> In our experiment, the high-rate of phagocytosis was observed mainly during 3 to 14 days after RD. At 14 days after RD, the thickness of PR and OS significantly decreased, in accordance with the previous report,<sup>46</sup> along with the reduced number of microglia. We suggested that the appropriate time to investigate the phagocytic effects of microglia has to be the point before significant loss of PR and OS.

In our study, the subretinal microglia exhibited two characteristics of phagocytosis: colocalization with OS and upregulation of phagocytic markers. Phagocytosis refers to the sensing and uptake of particles larger than 0.5  $\mu\text{m}$ .<sup>47</sup> The diameter of round OS debris in the SRS is around 2  $\mu\text{m}$  in our experiments (measurement based on hematoxylin and eosin staining), which serves as an idea size of particles for most efficient phagocytosis.<sup>47</sup> We detected several phagocytosis-related markers, including CD68, Dectin-1,<sup>48</sup> and DC-SIGN.<sup>49</sup> Immunoreactions of them were found in the subretinal microglia, not the microglia in the inner retina. CD68 is reported to be mostly localized in the late endosomes and lysosomes, with a small portion also expressed on the cell membrane to bind oxidized LDL and participate in phagocytosis.<sup>28,50</sup> Photoreceptor segment membranes are rich in cholesterol and lipids,<sup>51,52</sup> which may be a reason to activate CD68. Dectin-1 is a membrane-bound pattern recognition receptor that can directly recognize microbes and mediate phagocytosis.<sup>49</sup> Whereas DC-SIGN is recognized as another phagocytic receptor, as it is colocalized with phagosomes<sup>53</sup> and triggers Rho-GTPase.<sup>49,54</sup> Our data confirmed the upregulation of phagocytic markers in subretinal microglia, but further exploration is necessary to understand the precise mechanism of OS clearance. Furthermore, we presume that the removal rate of OS may not be constant after RD as the CD68+ iba-1+ cells decreased and CD68- iba-1+ cells increased with the progression of RD. The time for microglial infiltration and phagocytic efficiency may be limited and variable.

To explore whether microglia are essential to the removal of OS, PLX 3397 was applied to observe the morphology change of a detached retina without microglia. Our results demonstrate an interesting phenomenon: massive accumulation of OS in the SRS without microglial phagocytosis. Whether the generation of OS continues after RD remains

controversial. It is widely accepted that OS degenerates quickly after RD, but some studies suggest that disc addition is halted at the base after RD,<sup>55</sup> whereas other studies suggest that the new addition continues.<sup>56</sup> Our data supported that addition of OS still existed after RD, which required an alternative removal mechanism,<sup>23</sup> otherwise large deposits of OS could accumulate in the SRS. Although the death of PR decreased in the absence of microglia in the acute phase of RD, in the late phase, the thickness of PR without microglia was thinner than the retina with the presence of microglia, which indicates the potential protective role of microglia at the late stage of RD. PR did not benefit from the deposition of OS, as shown in our data, that there was no morphology and thickness recovery of PR in the long term. Previous reports have addressed the importance of OS clearance and homeostasis. The increase in OS absolute length and membrane assembly rates has a positive effect on retinal reattachment time.<sup>56</sup> A mathematical model also predicts that the removal rate of OS is a pivotal factor of the critical time within which the reattachment of retina can increase PR survival.<sup>23</sup> We saw the same thickening of the OS and hyper-reflective round lesions in the SRS in patients (see Fig. 7) as we did in the experimental RD model. We propose that the appropriate regulation of the state of OS addition and disposal may be an inelible issue in RD, which makes the understanding and mediating of the key phagocytes-microglia extremely important.

An unexpected phenomenon observed is that the ORU shown in the OCT image of patients with RD resembles the ruffled structure of outer retina in hematoxylin and eosin staining of RD mice treated with PLX3397, suggesting a potential correlation between accumulated OS in the SRS and ORU. The ORU, or outer retinal corrugations (ORCs), was described as a change in the outer retinal undulations (negative to positive) of  $\geq 3$  within a diameter of 6 mm[29], the presence of which was highly specific for RRD.<sup>57</sup> However, the ORU was debated about its possibility of predicting visual outcome.<sup>58–60</sup> Previous studies indicated that in the acute and subacute phases of RD (1–30 days after RD), ORU could be a prognostic indicator of bad vision, whereas ORU may be a good prognostic factor for vision when chronic cases are considered.<sup>29</sup> Another study suggests the persistent ORU after reattachment results in outer retinal folds, causing worse functional outcomes.<sup>61</sup> Given that the anatomic attachment without retinal displacement largely reflects the better vision outcome of patients,<sup>57,62</sup> the mechanism of ORU has raised great attention. Thus far, the potential mechanisms have included hydration of the interphotoreceptor matrix<sup>63</sup> and RPE-photoreceptor dysregulation theory.<sup>61</sup> The current hypothesis is derived from mathematical models and has not been verified in animal models. Our data may offer an alternative mechanism and contribute more insights to the current findings. Based on our hypothesis, in the acute phase, ORU may appear as an indication of OS accumulation as a result of insufficient phagocytosis, which accelerated the PR death. Therefore, the presence of ORU correlates with bad vision. During the chronic phase, ORU reflects a higher number of OS, which may indicate a higher survival rate of PR. Thus, more live PRs may be associated with a better vision outcome.

There are several limitations to this study. Iba-1 is expressed by microglia and macrophages in both ramified and reactive states,<sup>64</sup> making it challenging to iden-

tify the local microglia and infiltrating monocyte-derived macrophages in the SRS. In our study, more than 90% of the subretinal phagocytes were CD68-immunopositive at 3 and 7 days after RD. Because microglia and macrophages are both professional phagocytes in the CNS,<sup>65</sup> we did not subdivide the cell type. However, further exploration of the distinct function in different cell types is needed and necessary. Furthermore, we lack an effective tool to determine the optimal phagocytic efficiency required to protect PR. Besides, although we proposed a hypothesis of ORU, we cannot prove it in the clinic, as, for ethical reasons, there is no possibility to eliminate microglia in patients. In addition, we also lack the tools to evaluate the phagocytic capacity of microglia in living people. Additionally, the clinic discovery may be sporadic. Therefore, a well-designed clinical observational study with large samples is needed to prove the hypothesis.

In conclusion, our study revealed the important role of microglial phagocytosis in the clearance of OS. Insufficient removal of OS may lead to accumulation of deposits and distorted PR after long-term RD. Continued work on the regulation of the microglial phagocytosis will help define the mechanisms by which they can be exploited therapeutically to improve PR survival in patients with RD.

### Acknowledgments

**Author Contributions:** M.C. designed the experiments and wrote the manuscript. Y.Z. analyzed and interpreted data. M.C., Y.Z., Y.L., X.Z., and M.M. conducted the experiments. Y.Z., Y.L., X.Z., and M.M. provided materials. Y.L., X.Z., and M.M. proof-read and revised the manuscript. All the authors read and approved the final version of the manuscript and agree to be held accountable for all aspects of the work.

**Disclosure:** M. Cao, None; Y. Zhang, None; Y. Li, None; X. Zhang, None; M. Ma, None

### References

- Maidana DE, Gonzalez-Buendia L, Pastor-Puente S, et al. Peripheral monocytes and neutrophils promote photoreceptor cell death in an experimental retinal detachment model. *Cell Death Dis.* 2023;14(12):834.
- Cao M, Huang X, Zou J, et al. Attenuation of microglial activation and pyroptosis by inhibition of P2 × 7 pathway promotes photoreceptor survival in experimental retinal detachment. *Invest Ophthalmol Vis Sci.* 2023;64(7):34.
- Gao W, Du J, Chi Y, Zhu R, Gao X, Yang L. Minocycline prevents the inflammatory response after retinal detachment, where microglia phenotypes being regulated through A20. *Exp Eye Res.* 2021;203:108403.
- Kiang L, Ross BX, Yao J, et al. Vitreous cytokine expression and a murine model suggest a key role of microglia in the inflammatory response to retinal detachment. *Invest Ophthalmol Vis Sci.* 2018;59(8):3767–3778.
- Kataoka K, Matsumoto H, Kaneko H, et al. Macrophage- and RIP3-dependent inflammasome activation exacerbates retinal detachment-induced photoreceptor cell death. *Cell Death Dis.* 2015;6(4):e1731.
- Okunuki Y, Mukai R, Pearsall EA, et al. Microglia inhibit photoreceptor cell death and regulate immune cell infiltration in response to retinal detachment. *Proc Natl Acad Sci USA.* 2018;115(27):E6264–E6273.
- Janda E, Boi L, Carta AR. Microglial phagocytosis and its regulation: a therapeutic target in Parkinson's disease? *Front Mol Neurosci.* 2018;11:144.

8. Butler CA, Popescu AS, Kitchener EJA, Allendorf DH, Puigdemívol M, Brown GC. Microglial phagocytosis of neurons in neurodegeneration, and its regulation. *J Neurochem.* 2021;158(3):621–639.
9. Podleśny-Drabiniok A, Marcora E, Goate AM. Microglial phagocytosis: a disease-associated process emerging from alzheimer's disease genetics. *Trends Neurosci.* 2020;43(12):965–979.
10. Guo L, Choi S, Bikkannavar P, Cordeiro MF. Microglia: key players in retinal ageing and neurodegeneration. *Front Cell Neurosci.* 2022;16:804782.
11. Shobin E, Bowley MP, Estrada LI, et al. Microglia activation and phagocytosis: relationship with aging and cognitive impairment in the rhesus monkey. *Geroscience.* 2017;39(2):199–220.
12. Hollyfield JG, Perez VL, Salomon RG. A hapten generated from an oxidation fragment of docosahexaenoic acid is sufficient to initiate age-related macular degeneration. *Mol Neurobiol.* 2010;41(2–3):290–298.
13. Rashid K, Akhtar-Schaefer I, Langmann T. Microglia in retinal degeneration. *Front Immunol.* 2019;10:1975.
14. Goldberg AF, Moritz OL, Williams DS. Molecular basis for photoreceptor outer segment architecture. *Prog Retin Eye Res.* 2016;55:52–81.
15. LaVail MM. Kinetics of rod outer segment renewal in the developing mouse retina. *J Cell Biol.* 1973;58(3):650–661.
16. Young RW. The renewal of photoreceptor cell outer segments. *J Cell Biol.* 1967;33(1):61–72.
17. Hollyfield JG, Basinger SF. Photoreceptor shedding can be initiated within the eye. *Nature.* 1978;274(5673):794–796.
18. Kwon W, Freeman SA. Phagocytosis by the retinal pigment epithelium: recognition, resolution, recycling. *Front Immunol.* 2020;11:604205.
19. Wickham L, Lewis GP, Charteris DG, Fisher SK. Cellular effects of detachment and reattachment on the neural retina and the retinal pigment epithelium. *Retina.* 2013;29:605–617.
20. Lewis GP, Sethi CS, Linberg KA, Charteris DG, Fisher SK. Experimental retinal reattachment: a new perspective. *Mol Neurobiol.* 2003;28(2):159–175.
21. Johnson NF, Foulds WS. Observations on the retinal pigment epithelium and retinal macrophages in experimental retinal detachment. *Br J Ophthalmol.* 1977;61(9):564–572.
22. Anderson DH, Stern WH, Fisher SK, Erickson PA, Borgula GA. Retinal detachment in the cat: the pigment epithelial-photoreceptor interface. *Invest Ophthalmol Vis Sci.* 1983;24(7):906–926.
23. Annan WE, Asamani EOA, White D. Mathematical model for rod outer segment dynamics during retinal detachment. *PLoS One.* 2024;19(6):e0297419.
24. Zhang X, Henneman NF, Girardot PE, et al. Systemic treatment with nicotinamide riboside is protective in a mouse model of light-induced retinal degeneration. *Invest Ophthalmol Vis Sci.* 2020;61(10):47.
25. Young K, Morrison H. Quantifying microglia morphology from photomicrographs of immunohistochemistry prepared tissue using ImageJ. *J Vis Exp.* 2018;136:57648.
26. Abcouwer SF, Miglioranza Scavuzzi B, Kish PE, et al. The mouse retinal pigment epithelium mounts an innate immune defense response following retinal detachment. *J Neuroinflammation.* 2024;21(1):74.
27. Uribe-Querol E, Rosales C. Phagocytosis: our current understanding of a universal biological process. *Front Immunol.* 2020;11:1066.
28. Chistiakov DA, Killingsworth MC, Myasoedova VA, Orekhov AN, Bobryshev YV. CD68/macrosialin: not just a histochemical marker. *Lab Invest.* 2017;97(1):4–13.
29. Yeo YD, Kim YC. Significance of outer retinal undulation on preoperative optical coherence tomography in rhegmatogenous retinal detachment. *Sci Rep.* 2020;10(1):15747.
30. Wang Y, Zhao X, Gao M, et al. Myosin 1f-mediated activation of microglia contributes to the photoreceptor degeneration in a mouse model of retinal detachment. *Cell Death Dis.* 2021;12(10):926.
31. Lu W, Bhasin M, Tsirka SE. Involvement of tissue plasminogen activator in onset and effector phases of experimental allergic encephalomyelitis. *J Neurosci.* 2002;22(24):10781–10789.
32. Geloso MC, Corvino V, Marchese E, Serrano A, Michetti F, D'Ambrosi N. The dual role of microglia in ALS: mechanisms and therapeutic approaches. *Front Aging Neurosci.* 2017;9:242.
33. Bernardino L, Volonté C, Passani MB, Ferreira R. Editorial: Dual role of microglia in health and disease: pushing the balance towards repair. *Front Cell Neurosci.* 2020;14:259.
34. Haruwaka K, Ikegami A, Tachibana Y, et al. Dual microglia effects on blood brain barrier permeability induced by systemic inflammation. *Nat Commun.* 2019;10(1):5816.
35. Vidal-Itriago A, Radford RAW, Aramideh JA, et al. Microglia morphophysiological diversity and its implications for the CNS. *Front Immunol.* 2022;13:997786.
36. Green TRF, Rowe RK. Quantifying microglial morphology: an insight into function. *Clin Exp Immunol.* 2024;216(3):221–229.
37. Ling EA, Wong WC. The origin and nature of ramified and amoeboid microglia: a historical review and current concepts. *Glia.* 1993;7(1):9–18.
38. Davalos D, Grutzendler J, Yang G, et al. ATP mediates rapid microglial response to local brain injury in vivo. *Nat Neurosci.* 2005;8(6):752–758.
39. Xu YJ, Au NPB, Ma CHE. Functional and phenotypic diversity of microglia: implication for microglia-based therapies for Alzheimer's disease. *Front Aging Neurosci.* 2022;14:896852.
40. Zhao L, Zabel MK, Wang X, et al. Microglial phagocytosis of living photoreceptors contributes to inherited retinal degeneration. *EMBO Mol Med.* 2015;7(9):1179–1197.
41. Young RW. The renewal of rod and cone outer segments in the rhesus monkey. *J Cell Biol.* 1971;49(2):303–318.
42. Boesze-Battaglia K, Goldberg AFX. Photoreceptor renewal: a role for peripherin/rds. *Int Rev Cytol.* 2002;217:183–225.
43. Young RW, Bok D. Participation of the retinal pigment epithelium in the rod outer segment renewal process. *J Cell Biol.* 1969;42(2):392–403.
44. Vargas JA, Finnemann SC. Probing photoreceptor outer segment phagocytosis by the RPE in vivo: models and methodologies. *Int J Mol Sci.* 2022;23(7):3661.
45. Merriman DK, Sajdak BS, Li W, Jones BW. Seasonal and post-trauma remodeling in cone-dominant ground squirrel retina. *Exp Eye Res.* 2016;150:90–105.
46. Maidana DE, Gonzalez-Buendia L, Miller JW, Vavvas DG. Local photoreceptor cell death differences in the murine model of retinal detachment. *Sci Rep.* 2021;11(1):18798.
47. Baranov MV, Kumar M, Sacanna S, Thutupalli S, van den Bogaart G. Modulation of immune responses by particle size and shape. *Front Immunol.* 2021;11:607945.
48. Mata-Martínez P, Bergón-Gutiérrez M, Del Fresno C. Dectin-1 signaling update: new perspectives for trained immunity. *Front Immunol.* 2022;13:812148.
49. Kerrigan AM, Brown GD. C-type lectins and phagocytosis. *Immunobiology.* 2009;214(7):562–575.
50. Ramprasad MP, Terpstra V, Kondratenko N, Quehenberger O, Steinberg D. Cell surface expression of mouse

- macrosialin and human CD68 and their role as macrophage receptors for oxidized low density lipoprotein. *Proc Natl Acad Sci USA*. 1996;93(25):14833–14838.
51. Albert AD, Boesze-Battaglia K. The role of cholesterol in rod outer segment membranes. *Prog Lipid Res*. 2005;44(2–3):99–124.
52. Mitry D, Constable I, Singh J. Photoreceptor outer segment glaucoma in rhegmatogenous retinal detachment. *Arch Ophthalmol*. 2009;127(8):1053–1054.
53. Cambi A, Netea MG, Mora-Montes HM, et al. Dendritic cell interaction with *Candida albicans* critically depends on N-linked mannan. *J Biol Chem*. 2008;283(29):20590–20599.
54. Hodges A, Sharrocks K, Edelmann M, et al. Activation of the lectin DC-SIGN induces an immature dendritic cell phenotype triggering Rho-GTPase activity required for HIV-1 replication. *Nat Immunol*. 2007;8(6):569–577.
55. Lewis GP, Guérin CJ, Anderson DH, Matsumoto B, Fisher SK. Rapid changes in the expression of glial cell proteins caused by experimental retinal detachment. *Am J Ophthalmol*. 1994;118(3):368–376.
56. Guérin CJ, Lewis GP, Fisher SK, Anderson DH. Recovery of photoreceptor outer segment length and analysis of membrane assembly rates in regenerating primate photoreceptor outer segments. *Invest Ophthalmol Vis Sci*. 1993;34(1):175–183.
57. Oquendo PL, Sodhi GS, Naidu SC, et al. Optical coherence tomography features in fovea-off exudative vs rhegmatogenous retinal detachment. *Am J Ophthalmol*. 2024;268:212–221.
58. Cho M, Witmer MT, Favarone G, Chan RP, D'Amico DJ, Kiss S. Optical coherence tomography predicts visual outcome in macula-involving rhegmatogenous retinal detachment. *Clin Ophthalmol*. 2012;6:91–96.
59. Kang HM, Lee SC, Lee CS. Association of spectral-domain optical coherence tomography findings with visual outcome of macula-off rhegmatogenous retinal detachment surgery. *Ophthalmologica*. 2015;234(2):83–90.
60. Hagimura N, Suto K, Iida T, Kishi S. Optical coherence tomography of the neurosensory retina in rhegmatogenous retinal detachment. *Am J Ophthalmol*. 2000;129(2):186–190.
61. Muni RH, Darabad MN, Oquendo PL, et al. Outer retinal corrugations in rhegmatogenous retinal detachment: the retinal pigment epithelium-photoreceptor dysregulation theory. *Am J Ophthalmol*. 2023;245:14–24.
62. Lee WW, Francisconi CLM, Marafon SB, et al. Imaging predictors of functional outcomes after rhegmatogenous retinal detachment repair. *Retina*. 2024;44(10):1758–1765.
63. Dalvin LA, Spaide RF, Yannuzzi LA, Freund KB, Pulido JS. Hydration folds in rhegmatogenous retinal detachment. *Retin Cases Brief Rep*. 2020;14(4):355–359.
64. González Ibanez F, Picard K, Bordeleau M, Sharma K, Bisht K, Tremblay MÈ. Erratum: Immunofluorescence staining using IBA1 and TMEM119 for microglial density, morphology and peripheral myeloid cell infiltration analysis in mouse brain [published correction appears in *J Vis Exp*. 2019;152:6449].
65. Yu F, Wang Y, Stetler AR, Leak RK, Hu X, Chen J. Phagocytic microglia and macrophages in brain injury and repair. *CNS Neurosci Ther*. 2022;28(9):1279–1293.